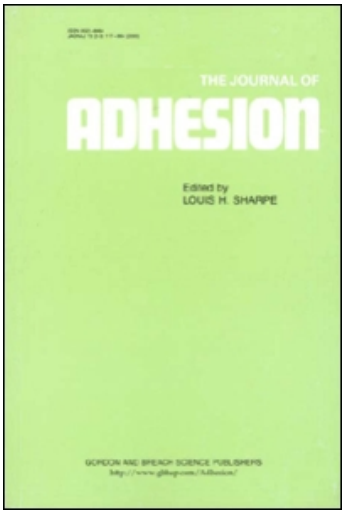

The Journal of Adhesion
Publication details, including instructions for authors and subscription information:
http://www.informaworld.com/smpp/title~content=t713453635

Polymer-Solid Interface Connectivity and Adhesion: Design of a Bio-Based Pressure Sensitive Adhesive

Richard P. Wool[a]; Shana P. Bunker[a]
[a] Department of Chemical Engineering, University of Delaware, Newark, Delaware, USA

To cite this Article Wool, Richard P. and Bunker, Shana P.(2007) 'Polymer-Solid Interface Connectivity and Adhesion: Design of a Bio-Based Pressure Sensitive Adhesive', The Journal of Adhesion, 83: 10, 907 — 926
To link to this Article: DOI: 10.1080/00218460701699773
URL: http://dx.doi.org/10.1080/00218460701699773

The Journal of Adhesion, 83:907–926, 2007

ISSN: 0021-8464 print/1545-5823 online
DOI: 10.1080/00218460701699773

Taylor & Francis
Taylor & Francis Group

Polymer-Solid Interface Connectivity and Adhesion: Design of a Bio-Based Pressure Sensitive Adhesive

Richard P. Wool
Shana P. Bunker
Department of Chemical Engineering, University of Delaware, Newark, Delaware, USA

Adhesion at polymer-solid interfaces was explored for a new bio-based pressure sensitive adhesive (PSA) in terms of sticker groups, ϕ_X, on the polymer phase, receptor groups, ϕ_Y, on the solid surface, and the bond strength of the sticker-receptor X-Y acid-base interaction, χ. The polymer-solid interface restructuring models of Gong and Lee et al. were extended with new percolation models of entanglements and interface strength to determine the optimal sticker group concentration, ϕ^*_X. For the general case where ϕ_Y and χ are constant, it is predicted that when $\phi_X < \phi^*_X$, that the critical peel energy behaves as $G_{1c} \sim \phi_X/\phi^*_X$ and the locus of failure is adhesive between the polymer and the solid. However, when $\phi_X > \phi^*_X$, failure occurs cohesively in a polymer-polymer interface adjacent to the solid and the strength decreases as $G_{1c} \sim \phi^*_X/\phi_X$. The switch from adhesive to cohesive failure can be understood in terms of the changes in the chain conformations of the adhered chains and their decreasing interpenetration, X_i, with the bulk chains, via $X_i \sim 1/r$, where $r = \chi\phi_X\phi_Y$. The optimal value of ϕ_X which maximizes the adhesion and determines the mode of failure is given by $\phi^*_X \approx 0.129/C_\infty$, and for typical values of the characteristic ratio C_∞ in the range 7–20, $\phi^*_X \approx 1\%$ mole fraction, corresponding to about 2 sticker groups per entanglement molecular weight, M_e. This result was verified for a bio-based PSA synthesized from an acrylated high oleic fatty acid, which was copolymerized with maleic anhydride as the sticker group. The observed behavior is counterintuitive to the current wisdom for the effect of acid-based interactions on adhesion, where the strength is expected to increase with the number of X-Y contacts. The surprisingly low value of $\phi^*_X \approx 1\%$ % sticker groups which maximizes the adhesion strength can now be readily calculated using the percolation model of entanglements and fracture.

Keywords: Bio-based; Entanglements; Fatty acids; Interface; Percolation; Polymer-solid; Pressure sensitive adhesives; Receptor groups; Sticker groups

Received 23 October 2006; in final form 30 July 2007.
One of a Collection of papers honoring Liliane Léger, the recipient in February 2007 of *The Adhesion Society Award for Excellence in Adhesion Science, Sponsored by 3M*.
Address correspondence to Richard P. Wool, Department of Chemical Engineering, University of Delaware, Newark, DE 19716, USA. E-mail: wool@udel.edu

1. INTRODUCTION

In adhesion applications, the polymer can be designed to incorporate functional groups that will result in optimal adhesive behavior, *i.e.* high peel energy and adhesive failure, for a given type of substrate. This article examines the effect of acid functional groups on the adhesive performance of a pressure sensitive adhesive (PSA) on a metal substrate. Currently, the majority of pressure sensitive adhesives are made from petroleum-based acrylate monomers, such as 2-ethylhexyl acrylate, n-butyl acrylate, and isooctyl acrylate. To alleviate this dependency on petroleum, it is desirable to investigate the synthesis and design of these adhesives from a renewable resource, such as plant oil. Plant oils are triglyceride esters of fatty acids, which vary in chain length and functionality. The most common plant oils have a carbon-carbon double bond functionality. Both triglycerides as well as individual fatty acids can be chemically modified in order to participate in free radical polymerization reactions [1,2]. Previous work by Bunker *et al.* in this area synthesized a monomer from a high oleic fatty acid methyl ester that is capable of forming high molecular weight polymers using an emulsion polymerization technique [3]. PSAs developed using this technology have shown similar properties to petroleum-based PSAs [4,5].

1.1. Polymer-Solid Adhesion: Background

Consider a linear polymer of molecular weight M adhering to a solid substrate, as shown in Figure 1. To promote adhesion, the polymer contains a mole fraction, ϕ_X, of sticker groups, X, which are attracted

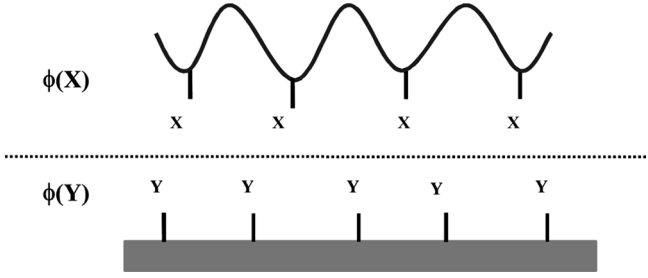

FIGURE 1 Schematic representation of the X-Y problem at a polymer-solid interface. X represents specific polymer sticker groups, Y represents specific substrate receptor groups, and ϕ is the mole percent or the mole fraction of the groups.

to the receptor groups, Y, on the substrate, where the areal coverage of the solid is ϕ_Y. The energy of interaction parameter, r, between the polymer and the solid can be expressed using the methods of Gong, Lee, and Wool [6–11]:

$$r \sim \chi\, \phi_X \phi_Y, \tag{1.1}$$

where χ is the strength of the X-Y acid-base type interaction. Common wisdom in the science of adhesion suggests that as we increase the number of X-Y acid-based interactions, that the polymer-solid adhesion energy increases as $G_{IC} \sim r$. However, this is not the case and it has been shown by Gong and Lee *et al.* [6–11] that the behavior is as depicted in Figure 2 where maximum values of r^* are observed. In

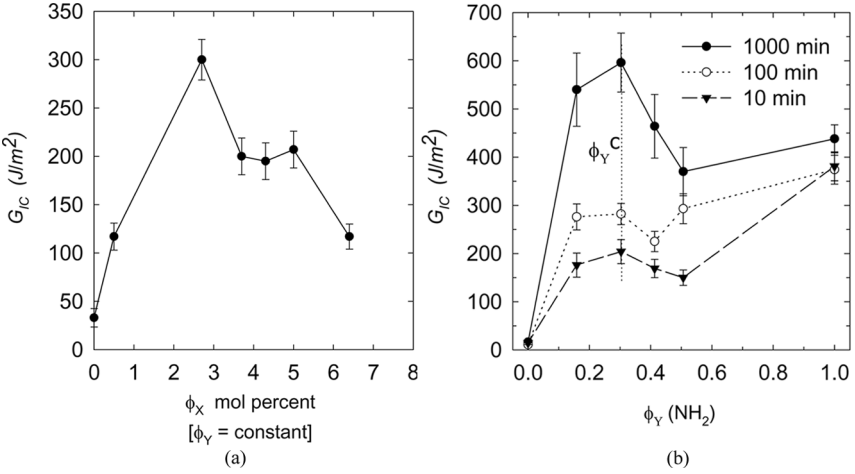

FIGURE 2 (a) Sticker group (X) effect on the fracture energy of a cPBD-Al interfaces. The M_w and M_n of the polymer were 180 k and 98 k, respectively. The samples were annealed at room temperature for 1000 min. The peeling rate of the samples was 30 mm/min. Copyright 1999 from "Adhension at Polymer-Solid Interfaces: Influences of Sticker Groups on Structure, Chain Connectivity and Strength," by Liezhong Gong and Richard P. Wool, *J. Adhesion* **71**, 189–209 (1999). Reproduced by permission of Taylor & Francis Group, LLC., http://www.informaworld.com. (b) Receptor Group (Y) effect on the fracture energy of a carboxylated polybutadiene aluminum silanated (cPBD-AlS) interfaces. The M_w and M_n of the polymer were 180 k and 98 k, respectively. The peeling rate of the samples was 30 min/min. The samples were annealed at room temperature for various times. On the AlS, $\phi_Y(-NH_2) + \phi_Y(-CH_3) = 1$. Here $\phi_X(-COOH)$ was about 3 mol%. The data point at $\phi_Y(-NH_2) = 0$ was based on the pure dispersive forces of PBD.

the first experiment by Gong *et al.* [8], the influence of ϕ_X on G_{IC} at constant $\phi_Y \sim 1$ was investigated. Carboxyl sticker groups were placed randomly on linear polybutadiene (PBD) chains and the polymer melt was adhered to aluminum (Al) foil surfaces. Pure PBD chains adhere very weakly to Al surfaces. The X-Y interaction was determined by the hydrogen bonding acid-base interaction between $-$COOH and aluminum oxide. It was found for this cPBD-Al interface that with increasing sticker group concentration, ϕ_X, the fracture energy G_{IC}, reached its maximum value of $300\,J/m^2$ at about $\phi^*_X = 3\%$ [Figure 2(a)].

In a related experiment by Gong and Wool [10], the influence of the Sticker-Receptor group bond strength, χ, was examined using aluminum oxide surfaces treated with amine terminated silanes, creating $-NH_2$ substrate receptor groups with a much stronger χ(X-Y) interaction. Then, the sticker concentration effect on the cPBD-AlS interface was investigated at constant $\phi_Y \sim 1$. It was found that similar trends to that shown in Figure 2(a) occurred but the maximum G_{IC} doubled to $600\,J/m^2$ and the optimal sticker concentration decreased to $\phi^*_X \sim 0.5\,mol\%$. Again, the failure mode was cohesive at high G_{IC} values and was purely adhesive near $\phi_X \ll \phi^*_X$.

Finally, the third experiment by Lee and Wool [6,7] varied the coverage of active amine receptor groups, ϕ_Y, in the range 0–100% on the aluminum surface using mixed silanes (–CH_3 and $-NH_2$ terminated). A cPBD polymer with a constant sticker group concentration $\phi_X = 3\,mol\%$, corresponding to ϕ^*_X in Figure 2(a), was used in the peel experiments. The results of G_{IC} *vs.* ϕ_Y are shown in Figure (2b) for surface restructuring times of 10, 100, and 1000 min. Significantly, G_{IC} reaches its maximum value of about $600\,J/m^2$ at an optimal partial coverage of $\phi^*_Y \sim 30\%$.

Similar optimal adhesion effects have been observed by Leger *et al.* [12–14] when adhering polymers to elastomers and silica substrates. For example, Deruelle *et al.* [14] examined the adhesion of a PDMS elastomer to a solid silicon substrate that contained an areal density, Σ, of grafted linear PDMS chains of varying molecular weight, M, which were compatible with the elastomer. They found an optimal areal density with higher molecular weight connectors that gave a maximum in the adhesion energy. These results could be interpreted in terms of sufficient interpenetration of the tethered chains into the elastomer network, which would be limited by swelling, as proposed by Brochard-Wyart *et al.* [15].

We have found for several polymer-solid interfaces that the locus of failure, cohesive or adhesive, depends on the optimal values of the sticker and receptor groups. A microscopic analysis of the mode of failure (AFM, XPS, SEM) indicated that cohesive failure was occurring

predominantly in a layer immediately adjacent to the metal surface. At low G_{IC} and ϕ_X values, simple adhesive or mixed adhesive-cohesive failure occurred. Thus, when $\phi_X < \phi^*_X$, and when $\phi_Y < \phi^*_Y$, then adhesive failure occurs at the polymer-solid interfaces and the polymer cleanly debonds from the solid, which is critical for the design of PSAs. However, when $\phi_X > \phi^*_X$ and $\phi_Y > \phi^*_Y$, we have shown that failure occurs cohesively at a polymer-polymer interface adjacent to the solid substrate [6–11]. Cohesive failure occurs in a depletion layer adjacent to the solid by virtue of the high adsorption of the sticker groups on the surface, as shown by Gong [11]. Angle Resolved XPS (ARXPS) was used on a model glassy system, PS-MA-SiO_2, where 7 mol% maleic anhydride was copolymerized with styrene and adsorbed above Tg on a SiO_2 substrate. The polymers had Mn values of 100 k Daltons and Mw values of 224 k Daltons. The polymer solid interface was equilibrated by annealing above T_g (125°C for 7 mol% MA and 132°C for 14%mol% MA) and then the free or weakly attached

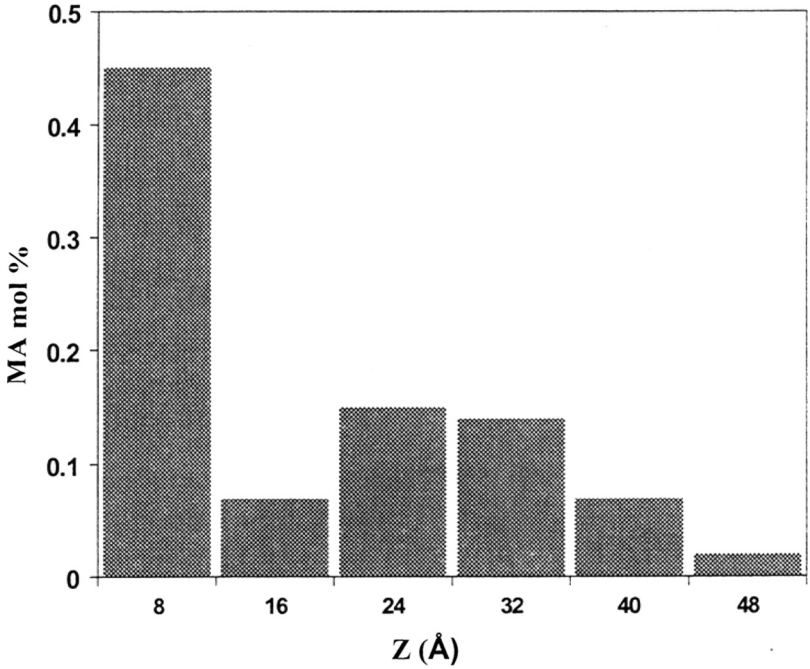

FIGURE 3 The concentration depth profile $\phi(Z)$ of MA groups for a polystyrene chains containing 0.14 mole maleic anhydride sticker groups attached to a SiO_2 substrate, as obtained by ARXPS. The non-attached chains were removed by solvent extraction.

chains were washed away with toluene and the resulting interface of adhered chains analyzed by ARXPS. The depth profile $\phi(Z)$ of MA (Figure 3) showed that the surface layer of MA at $\phi(Z) = 0$ in contact with the solid was about 3 times the average value (*e.g.* 14%) but there also existed MA depletion zones near $\phi(Z) = 20\,A$ and $\phi(Z) = 40\,A$ of the surface. This sticker group profile was consistent with a random walk chain making contact with a surface and beginning to flatten out by adsorption on the surface, thereby creating a strong adhesion at $\phi(Z) = 0$ but also creating a depleted entanglement zone resulting in low cohesive failure in the bulk adjacent to the solid. Gong's $\phi(Z)$ analysis was in accord with a Self Consistent Field Lattice Model (SCFLM) analysis of $\phi(Z)$ at polymer solid interfaces [9–11]. Thus, there are design rules for polymer-solid interface when sticker and receptor groups are involved. In this article we explore these rules in the light of advances in the understanding of fracture of polymer interfaces [16,17] and new theories of entanglements [17,18]. We apply the rules to the design of a new bio-based pressure sensitive adhesive, where the PSA was derived from a high oleic soybean oil, as described by Bunker *et al.* [3–5].

2. DESIGN RULES FOR POLYMER-SOLID INTERFACES

The adhesive fracture energy, G_{AD}, between adsorbed chains and the solid surface behaves as $G_{AD} \sim r$ [7,10] such that

$$G_{AD} \sim \chi\ \phi_X\ \phi_Y. \tag{2.1}$$

The adhesive stress, σ_{AD}, to adhesively debond in peel is given by [7,10],

$$\sigma_{AD} \sim r^{1/2}. \tag{2.2}$$

The above relations are in accord with the Nail solution for simple adhesive fracture of weak interfaces [19,20], and are comparable with the Velcro model suggested by McLeish [21] and the compatiblizer model (with chain length less than M_c) used for incompatible interfaces by Creton *et al.* [22,23].

As the chains adsorb strongly on the solid substrate with increasing r-values, they collapse their random coil dimensions on the solid substrate and disentangle themselves from their neighboring chains above, thereby creating a weak polymer-polymer interface. The interpenetration distance, X_i, between the adhered and the neighboring chains depends on $r = \chi\phi_X\,\phi_Y$ *via* the Entanglement Sink Probability

model suggested by Lee and Gong [7,10] as,

$$X_i \sim 1/r. \tag{2.3}$$

When the chains become attracted to the surface with increasing r-values, their conformations are perturbed such that their radius of gyration perpendicular to the surface decreases in accord with Eq. 2.3, subsequently decreasing the extent of interpenetration with the neighboring chains. Furthermore, the cohesive strength, G_{CO}, of a polymer-polymer interface with interpenetration distance X_i is derived from the rigidity percolation model [16,17] *via* $G_{CO} \sim [p\text{-}p_c]$, where, for any polymer-polymer interface, the percolation parameter, p, is related to the normalized entanglement density *via*.

$$p \sim \Sigma\, N/X_i. \tag{2.4}$$

Here Σ is the number of chains per unit area, $N \sim L/L_e$ is proportional to the number of entanglements per chain of contour length, L, with entanglement length, L_e, and X_i is the interpenetration distance corresponding to the width of the interface. If brush-like ordering occurs at an interface, then L_e increases significantly and N decreases towards a critical value creating a very weak interface. Similarly, for a partially interpenetrated interface, N decreases at the interface relative to its fully interpenetrated value and the interface strength decreases. This is the case for the weak layer adjacent to the solid surface in our analysis.

The polymer-polymer interface immediately adjacent to the solid substrate essentially behaves like an incompatible polymer-polymer interface described in [16], where $X_i \sim N^{1/2}$ and Σ is constant such that we obtain

$$G_C \sim [X_i - X_{ic}], \tag{2.5}$$

in which X_{ic} is a critical interpenetration distance related to the critical entanglement molecular weight M_c *via* $X_c \sim {M_c}^{1/2}$ and is related to the tube diameter of the entangled reptating chains. Thus, we expect that

$$G_{CO} \sim [1/r - 1/r_c], \tag{2.6}$$

in which $r_c \sim 1/X_c$. The critical stress, σ_{CO}, for cohesive failure is related to $r = \chi\phi_X\,\phi_Y$ *via*

$$\sigma_{CO} \sim [1/r - 1/r_c]^{1/2}. \tag{2.7}$$

In a peel experiment where the polymer is being debonded from the solid substrate, the behavior of the peel forces for cohesive and adhesive failure as a function of $r = \chi\ \phi_X\,\phi_Y$ is shown schematically in Figure 4. Note that the optimization is done with regard to stress and not fracture

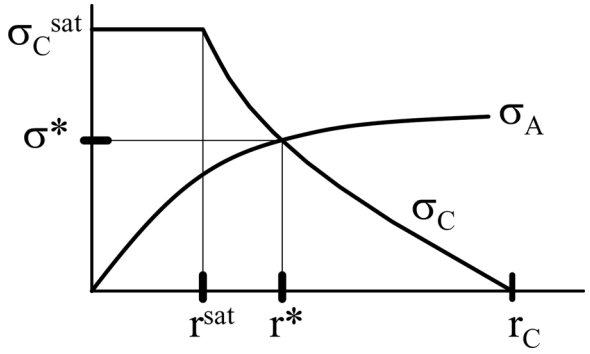

FIGURE 4 The crossover point of adhesive *vs*. cohesive failure stress at the critical value of $r^* = (\chi\phi_X\phi_Y)^*$.

energy of the adhesive and cohesive interfaces. When $\sigma_{CO} = \sigma_{AD}$, the model predicts maximum adhesion strength at an optimal value of $r^* = (\chi\phi_X\phi_Y)^*$. Thus, for a given χ value, there exists optimal values ϕ_X and ϕ_Y for the sticker and receptor groups, above or below which the fracture energy will not be optimized. Alternatively, if the X-Y interaction strength, χ, increases, the number of sticker groups required to achieve the optimum strength decreases. Significantly, the optimum strength is not obtained when the surface is completely covered with receptor groups ($\phi_Y = 1$) and is closer to 30%. For polybutadiene, the optimum value of r^* was determined experimentally, and typically $\phi_X \approx 1.0\%$ and $\phi_Y \approx 25\%$–30% [7].

To apply the above analysis to the design of a new polymer-solid interface, we consider first the most common polymer-solid interface in which $\phi_Y = 1$ (receptor groups totally cover the solid surface) and the polymer contains a variable amount of sticker groups, ϕ_X, as depicted in Figure 2. Thus, for this interface, we have $r^* = (\chi\phi_X)^*$. Since χ is constant, then $r \sim \phi_X$ and when $\phi_X < \phi^*_X$, the fracture energy $G_{1C} \sim r$ where adhesive failure dominates, and we obtain

$$G_{1C} = G_o + G^*_{1C}\phi_X/\phi^*_X \qquad (r < r^*), \tag{2.8}$$

in which $G_{1C}{}^*$ is related to the maximum fracture energy and G_o is the adhesion value at $\phi_X = 0$. In Figure 2, $G^*{}_{1C} \approx 300\,J/m^2$ at $\phi^*{}_X = 3\%$ and when $\phi_X \approx 1\%$, we predict a fracture energy of $G_{1C} \approx 100\,J/m^2$, as noted.

However, when $r > r^*$ or when $\phi_X > \phi^*{}_X$, cohesive failure dominates and using $G_{1C} \sim \sigma_{CO}{}^2 \sim [1/r - 1/r_c]$, we obtain

$$G_{1C} = G^*_{1C}[\phi^*_X/\phi_X - \phi^*_X/\phi_{XC}] \qquad (r > r^*), \tag{2.9}$$

where ϕ_{XC} is the critical value of ϕ_X when the polymer-polymer interface is marginally connected and very weak with interdiffusion distances of the order of R_{ge}. Since ϕ_{XC} is expected to be much greater than ϕ^*_X, we will neglect its contribution and focus on values of ϕ_X near ϕ^*_X. For example, in Figure 2, using $G_{1C} = G^*_{1C}\ \phi^*_X/\phi_X$, at $\phi_X = 6\%$, one expects that $G_{1C} \sim 1/2\, G^*_{1C}$, or about $150\,J/m^2$ as observed. One should be able to estimate ϕ_{XC} from the relation $\phi_{XC} = \phi^*_X\ R/h$, where R is the end-to end vector of the chain and $h = V/R^2$. When a random walk sphere collapses on a surface into a pancake shape by preserving its dimension in two directions, the thickness, h, is equivalent to the packing length parameter, P, discussed by Fetters *et al.* [24] for entanglements, and $V = M/\rho Na$ is the volume of the chain. This gives typical values for ϕ_{XC} which are about an order of magnitude greater than ϕ^*_X.

If the solid surface became contaminated such that ϕ_Y decreased from 100% to 80% coverage, then ϕ^*_X needs to be increased from 3% to 3.75% to obtain the same fracture energy. Therefore, with regard to sticker group variation, we see that the optimization "hill" shape is quite asymmetric due to the nature of adhesive ($G_{1C} \sim r$) vs. cohesive failure ($G_{1C} \sim 1/r$). Thus, when designing interfaces for optimal adhesion in which χ and ϕ_Y are constant, values of ϕ_X on the low side of ϕ^*_X can weaken the interface more than on the high side of ϕ^*_X.

The optimal sticker group value, ϕ^*_X, can be deduced from the percolation model of entanglements [18,20] shown in Figure 5, where the critical entanglement molecular weight, M_c, is determined when the chain is of sufficient length to cross an arbitrary plane three times. If the number of chains per unit area is Σ and the cross-section of a chain segment in the bulk is a, then the critical condition is met when $3a\Sigma = 1$. For the polymer-solid interface, we place a sticker group on the solid and begin a random walk and inquire using "coin-toss" statistics when that chain will return to the surface. In an entangled melt, a polymer chain segment of molecular weight M_c crosses any arbitrary plane three times, which is about half the number of times it returns to the plane. Thus, the entanglement molecular weight M_e is about half that of the critical entanglement molecular weight M_c. We find that this occurs after about $N_c \approx 30$ random walk steps and the entanglement molecular weight M_e is given by [18]:

$$M_e \approx 31 C_\infty M_j \qquad (3/1 \text{ helices}) \quad \text{and} \tag{2.10}$$

$$M_e \approx 22 C_\infty M_j \qquad (2/1 \text{helices}), \tag{2.11}$$

in which C_∞ is the characteristic ratio of the random walk and M_j is the molecular weight per bond, *e.g.*, $M_j = 14\,g/mol$ for polyethylene and

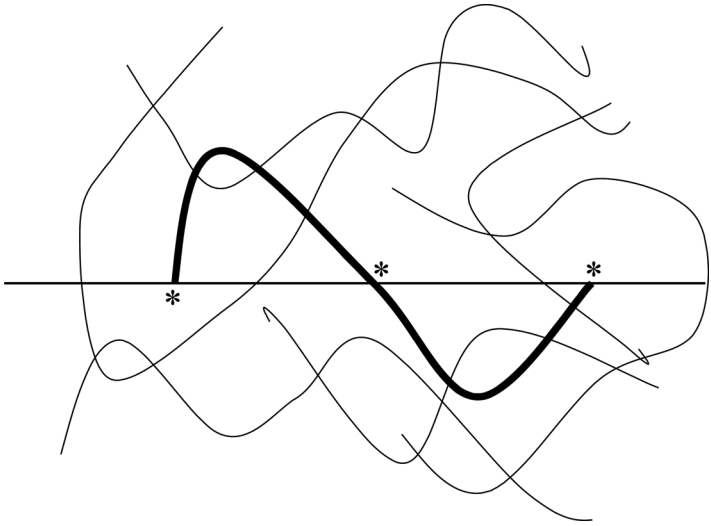

FIGURE 5 The entanglement molecular weight M_c (bold) is shown schematically as a random walk which is long enough to cross a plane three times, as predicted by the Entanglement percolation Model. The entanglement molecular weight M_e is about half of M_c.

52 g/mol for polystyrene. The front factor of 31 is used for 3/1 helices *e.g.*, Polystyrene (PS), Poly (methyl methacrylate) (PMMA), Poly (vinyl chloride) (PVC), Poly (vinyl acetate) (PVA), etc.), and is 22 for 2/1 helices (planar zig-zag structure, PE, polyamides, alkane-esters etc.). This value depends on the local conformational details of the chain cross-section, a, as discussed in [18,20]. Thus, to adhere an entanglement network to a solid, we place a sticker group at every "return touch point" of the random walk on the substrate, or on average, about two groups per M_e value, such that the optimal mole fraction of sticker groups is given by

$$\phi_X^* = 2j\ M_j/M_e, \tag{2.12}$$

in which $M_j = M_o/j$, where j is the number of backbone steps per monomer of molecular weight M_o. Substituting for M_c in the latter equation, and using $j = 2$, we obtain the optimal mole fraction of sticker groups as

$$\phi_X^* \approx 0.129/C_\infty \qquad (3/1\,\text{helices}) \quad \text{and} \tag{2.13}$$

$$\phi_X^* \approx 0.0.178/C_\infty \qquad (2/1\,\text{helices}). \tag{2.14}$$

The characteristic ratio, C_∞, is heavily dependent on the bond molecular weight, M_j. It has been shown that for homologous series of

polymers of the 3/1 helical type $-CH_2-CHX-$, where X is the variable side group, that C_∞ depends on M_j as[1]:

$$C_\infty = 1.36\, M_j^{1/2}. \tag{2.15}$$

Substituting the latter relation in Eq. 2.10, one obtains a very simple approximation for M_e and M_c for 3/1 type polymers as:

$$M_e \approx 42\, M_j^{3/2} \text{g/mol} \quad \text{and} \tag{2.16}$$

$$M_c \approx 84\, M_j^{3/2}\ \text{g/mol}. \tag{2.17}$$

For example, with polystyrene, $M_j = 52$ g/mol and we predict that $M_c \approx 31{,}500$ g/mol, which is in accord with experimental values with $M_c \approx 30{,}000$ g/mol [24]. Since many polymers have C_∞ values in the range of 5–20 and $j = 2$ for vinyl polymers, it appears that there is an optimal sticker group number of $\phi^*_X \approx 1$–2%, which is a surprisingly small number to maximize adhesion. These relations will be explored further in the following sections and demonstrated by experimental data.

3. EXPERIMENTAL

3.1. Materials

The bio-based monomer, acrylated oleic methyl ester (AOME) was synthesized using methods previously reported [3–5]. A schematic of this process is shown in Scheme 1. The emulsifier sodium lauryl sulfate (SLS) (10 wt.% aqueous solution) (Aldrich, Milwaukee, WI) and the initiator 2,2′-azobis(2-methylbutyronitrile) (Vazo 67, Dupont, Wilmington, DE) were used as received. Reagent grade methyl methacrylate (Aldrich) and maleic acid (MA, Aldrich) was also used as received. An additional initiator, 2,2′ azobis(2-amidinopropane) dihydrochloride (V-50, Wako Pure Chemical Industries, Osaka, Japan) was used as received.

The polymers were synthesized using miniemulsion polymerization as previously reported [3,4]. In each miniemulsion polymerization, 9 g AOME, 1 g methyl methacrylate, 0.03 g Vazo 67, 2 g SLS (10% aq. solution), and 40 g water were used. The quantity of MA was varied for each experiment as shown in Table 1. In addition, 0.003 g of the water-soluble initiator, V-50, was used to aid in the initiation of the

[1]R. P. Wool, Presented at the American Physical Society Annual Meeting, March 2007.

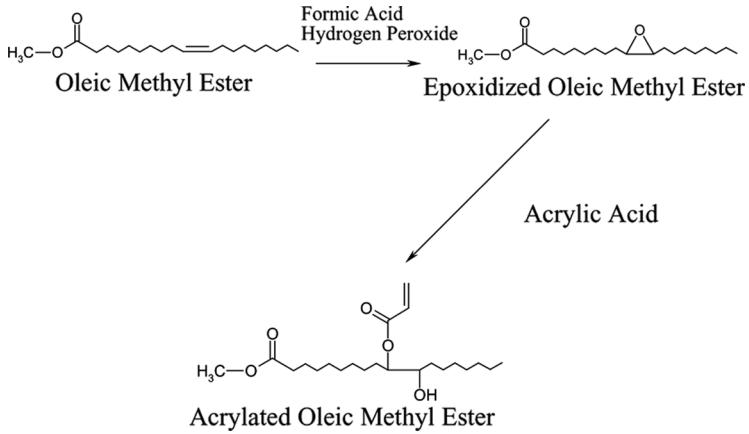

SCHEME 1 Diagram of the monomer synthesis steps.

MA that will preferentially reside in the aqueous phase. For viscoelastic and adhesive testing, the polymers were obtained from the dispersions by simply evaporating the water.

3.2. Dynamic Mechanical Analysis (DMA)

The rheological tests were conducted on a Rheometrics ARES, Union NJ, using a 25 mm cone and plate geometry (angle = 0.0998 radians) with a frequency of 6.2 rad/sec, and a strain of 1%. Strain sweep tests, at a constant frequency and temperature, were performed to confirm that a 1% strain is in the linear viscoelastic region. Viscoelastic properties were measured at temperatures in the range of -20°C to 95°C at a step temperature of 5°C.

TABLE 1 The Quantity of Maleic Acid (MA) Added to Different Polymerization Reactions

Sample	Mol% MA	Weight of MA in polymerization (g)
1	0.5	0.02
2	0.75	0.03
3	1	0.036
4	1.25	0.049
5	1.5	0.06

3.3. Adhesion Characterization

The adhesive films were applied to an aluminum sheet (0.001" thickness, Precision Brand, Inc., Downers Grove, IL) using a 400 μm doctor blade. The water from the latex evaporated in ambient conditions yielding a film thickness of 80 μm, nominally. The substrate for these tests was a stainless steel plate. The substrate was prepared by cleaning with ethyl acetate, which removed any contaminants on the plate. The plate was subsequently cleaned with acetone. The peel adhesion samples, approximately 25 mm in width and 100 mm in length, were adhered to the plate using a 2 kg roller. The roller was "rolled" over the adhesive samples four times at a rate of approximately 1 cm/sec. The samples were adhered to the stainless steel plate using a 2 kg roller in the same manner as the peel samples [7]. The peel strength of the adhesives was analyzed using a 180° peel test in accordance with ASTM D903[7]. The tensile testing machine was a Mini-Instron 44 (Canton, OH). The speed of the crosshead was 300 mm/min. The samples were tested at ambient temperature and humidity, approximately 22°C and 50% relative humidity. The peel energy can be calculated using:

$$G_{1c} = \frac{2P}{b}, \tag{3.1}$$

where G_{1c} is the peel energy, P is the peel force, and b is the width of the sample.

3.4. Acid Number

The acid number is a value describing the total acidity of a polymer. ASTM D 1994–91 was used to determine the acid number of the polymers that contained MA. In this technique, a potassium hydroxide/methanol titrant was used with a phenolphthalein indicating solution (~2.5 g/L). To determine the exact normality of the methanolic KOH solution, a standard acid solution of potassium hydrogen phthalate was used and the normality is calculated as:

$$\text{NKOH} = \frac{\text{g of phthalate}}{\text{mL of KOH solution}} \times 4.90. \tag{3.2}$$

The normality of the titrant used in this work was 0.08 N. Approximately 2 grams of polymer was dissolved in 200 mL of toluene by heating the solution to 85°C. After the polymer was fully dissolved, the temperature was decreased to 55°C and the indicating solution was added. The sample was titrated until a light pink color was maintained for at least 10 seconds. The acid number is calculated by

the following:

$$\text{acid}\#(\text{mg KOH/g sample}) = \frac{(\text{mL KOH sol'n}) \times (\text{KOH Normality}) \times 56.1}{\text{grams of adhesive}}. \tag{3.3}$$

To remove free MA from the polymer sample, the polymer was washed three times with both methanol and water prior to titration. This technique will allow a comparison between polymer samples with different quantities of MA. Each acid number was repeated three times and a standard deviation was calculated.

4. RESULTS AND DISCUSSION

4.1. Acid Number

Figure 6 shows the increase in acid number with the increase in MA added in the initial monomer mixture. This indicates that the MA is being incorporated into the polymer backbone. However, the magnitude of the acid number is higher than expected for a given quantity of acid initially charged to the reaction vessel. Partial hydrolysis of the methyl methacrylate and AOME monomers could account for this higher than expected for a given quantity of acid initially charged to the reaction vessel. Partial hydrolysis of the methyl methacrylate and AOME monomers

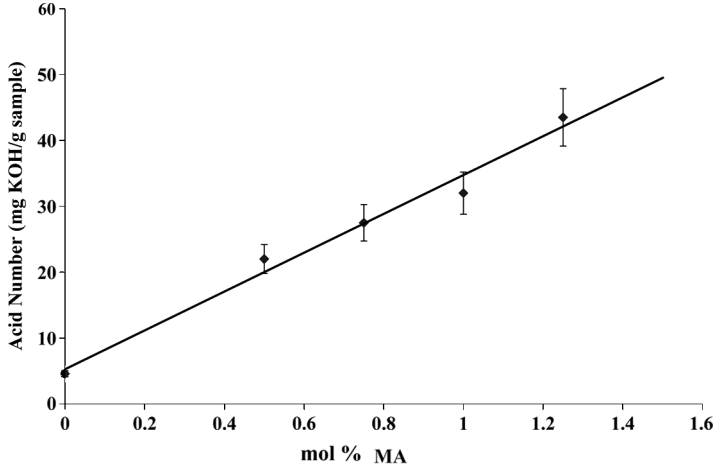

FIGURE 6 The experimentally recorded acid number as a function of MA added to the monomer mixture.

could account for this higher than expected value, however, the increasing trend confirms the incorporation of MA into the polymer. The range of MA incorporation into the PSA was 0–1.3 mol%.

4.2. Viscoelastic Properties

The storage modulus as a function of temperature at six different MA concentrations (as shown in Figure 5) is shown in Figure 7. These are compared with the storage modulus of a miniemulsion polymer that contains no MA shown underneath. With increasing MA content, the storage moduli of the AOME-co-MMA-co-MA polymers increase slightly and monotonically compared with the AOME-co-MMA polymer. This is attributed to the stiffer MA group that is incorporated into the polymer chain. It is significant to note that while the viscoelastic properties show the expected small increase with MA content, that this trend will not be able to predict the non-monotonic adhesion effects, comparable with the trends in Figures 2 and 3. Furthermore, the adhesion behavior cannot be explained by changes in bulk viscoelastic energy dissipation.

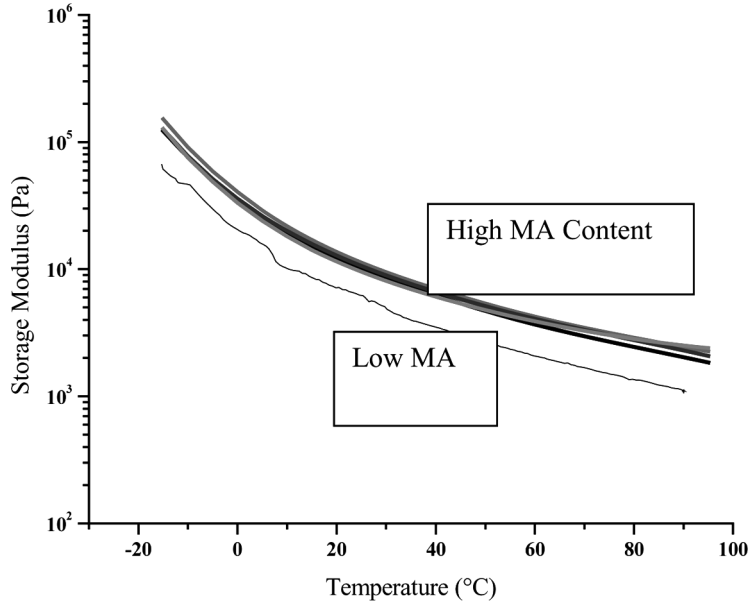

FIGURE 7 The storage modulus G′ of the polymers that contain MA as a function of temperature. The thin line (bottom) represents a comparable polymer that contains no MA and the increasing MA polymers are on top.

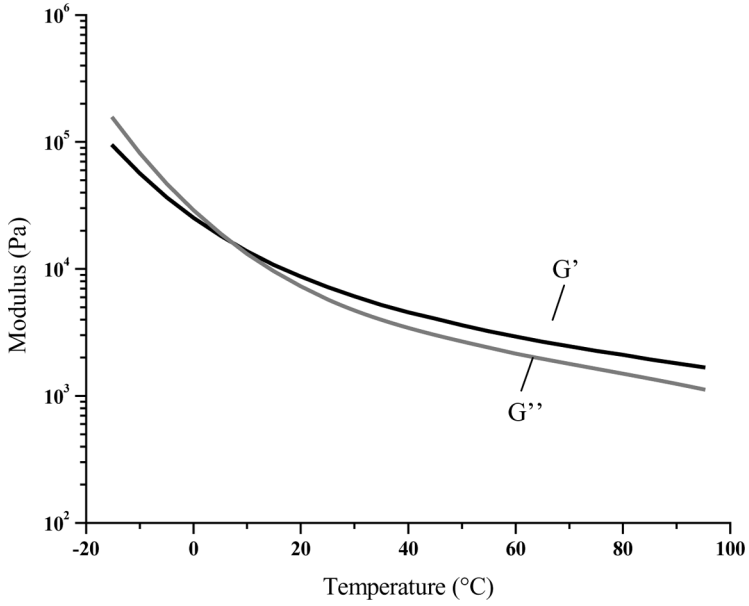

FIGURE 8 The storage and loss modulus of an AOME-co-MMA-co-MA polymer.

An example of the storage and loss modulus of an AOME-co-MMA-co-MA polymer is shown in Figure 8. The G′ is greater than the G″ at temperatures greater than 0°C, which indicates that the elastic behavior of the polymer dominates the properties and that physical entanglements are present. Similar behavior is observed for all of the polymers synthesized with MA. The G′ values can be used to estimate the entanglement molecular weights, M_e, of the PSA using rubber elasticity theory, $M_e = 4/5\ kT/G'$, where ρ is the density, k is Boltzmann's constant, and T is the temperature in degrees Kelvin. For example, at $T = 373\,K$, $\rho \approx 0.8\,g/cc$, and $G' \approx 2{,}000\,N/m^2$ such that we obtain $M_e \approx 99{,}000\,g/mol$ and $M_c \approx 200{,}000\,g/mol$. Using Eq. (2.12), the optimal value of $\phi^*_X = 0.7\%$ would be obtained with $M_j = 178\,g/mol$ and $j = 2$, which is comparable with that shown in Figures 2 and 3 for the carboxylated butadiene PSA. This observation is further explored in the next section with regard to adhesive properties.

4.3. Adhesion Properties

The increase in peel energy with the increase in MA content is shown in Figure 9. The peel energy increases linearly to an optimum

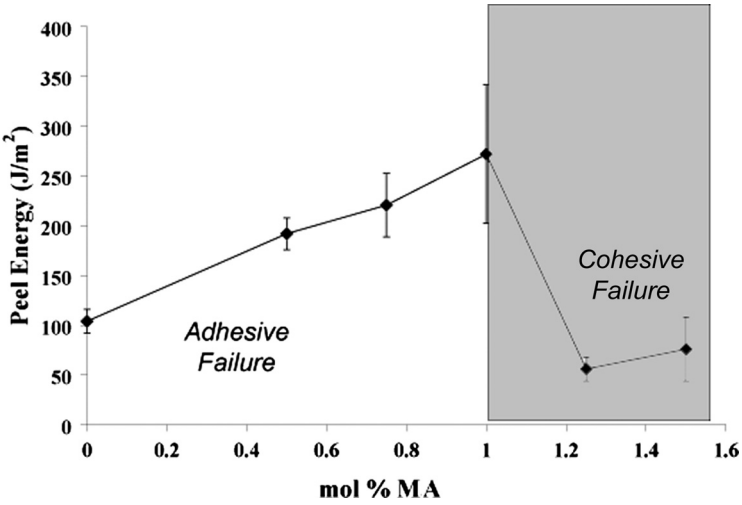

FIGURE 9 The peel energy as a function of MA content ϕ_X. An optimum concentration ϕ^*_X of approximately 1 mol% MA results in high peel energy and adhesive failure.

concentration of MA, at approximately $\phi_X^* \approx 1\,\text{mol}\%$, with adhesive failure. In the adhesive failure region at $\phi_X < \phi^*_X$, the peel strength is well described by Eq. 2.8 as

$$G_{1C} = 110 + 140\phi_X/\phi_X^* \; [J/m^2], \tag{4.1}$$

in which $G_o = 110\,J/m^2$ at $\phi_X = 0$ and $G^*_{IC} = 140\,J/m^2$. When $\phi_X > \phi^*_X$, Eq. 2.9 predicts that

$$G_{1C} = 250\ \phi_X^* \; [1/\phi_X - 1/\phi_{XC}]. \tag{4.2}$$

Typically, the transition from adhesive to cohesive failure is not smooth at ϕ^*_X and an exact comparison of theory with the experimental decrease in G_{IC} using the latter equation is not useful in this case. Suffice to say that a significant decrease in G_{IC} values are noted at $\phi_X > \phi^*_X$ which accompanies the transition from adhesive to cohesive failure.

At 1 mol% MA, a very small amount of cohesive failure 'patches' were observed. Specifically, randomly located small quantities of adhesive were observed on the stainless steel substrate. Therefore, the optimum level of MA is slightly below 1 mol%. This result is in excellent agreement with the predicted value of $\phi_X^* \approx 1.0\%$ as given by Eq. 2.13. Because this polymer has three monomers, a weighted average monomer molecular weight, M_o, is calculated as follows:

$$\overline{M_o} = x_1 M_{o1} + x_2 M_{o2} + x_3 M_{o3}, \tag{4.3}$$

where x_x is the weight fraction of the corresponding monomer. Based on the extreme cases of the terpolymer (0.5 mol% and 1.5 mol% MA, the quantity of AOME and MMA remained fixed), then $\overline{M_o}$ is 356 g/mol and $M_j = 178$ g/mol. Using Eq. 2.15, we obtain $C_\infty \approx 18$. The M_e value can be calculated using the entanglement model (Eq. 2.10 for a 3/1 helix using $C_\infty = 18$) as $M_e = \approx 100{,}000$ g/mol. Alternatively, using $M_e = 42\, M_j^{3/2}$ (Eq. 2.16), we also obtain $M_e \approx 100{,}000$ g/mol, which is in excellent agreement with the M_e value obtained from the dynamical mechanical analysis. Subsequently, we obtain $\phi_x \approx 0.7$ % and this estimate is slightly less than the experimentally determined value of approximately 1%. An exact agreement with the 1% value would be obtained if $C_\infty = 13$ instead of $C_\infty = 18$ used in the calculation. The characteristic ratio for this polymer was not determined independently but these values are reasonable when compared with similar polymers.

Thus, we can summarize these unusual results in the following sequence of events: (a) A polymer consisting of interpenetrated random walk chains with $M \gg M_e$ containing sticker groups X makes contact with a solid surface containing receptor groups Y which enable an X-Y bond to form at the polymer-solid interface. (b) Thermodynamically driven surface restructuring occurs where the random walk chains begin to collapse *via* the X-Y attraction on the solid overcoming the entropy penalty for random coils, whereby the concentration of X groups increases at the solid surface, causing a depletion in the bulk. (c) With increasing attraction of the chains to the surface, the attached random walk chains disentangle from the non-attached layer above the surface, which creates a weak cohesive zone. (d) With increasing attractiveness of the chains to the solid, the adhesive strength continues to grow linearly with the number of X-Y bonds while the cohesive zone continues to weaken and, eventually, the cohesive zone becomes the weak link and the fracture mode changes from adhesive to cohesive. (e) The ideal or optimal situation for the chains involves little or no surface rearrangement such that when a random walk chain touches the surface, it has one sticker group per "touch" and is then free to entangle with the other chains above in the bulk. This corresponds to two sticker groups per M_e, which defines the optimal sticker concentration ϕ^*_X when $\phi_Y = 1$. Typically, $\phi^*_X \approx 1\%$ which presents some interesting design concepts for adhesives in general.

5. CONCLUSIONS

Carboxylic acid groups were added to the polymer backbone in order to enhance the adhesive performance of the plant-oil based PSA. MA sticker groups were incorporated into the polymer chain and the impact on the

viscoelastic properties of the resulting polymer was negligible. However, the peel energy increased 150% with the addition of only 1 mol% MA. In the adhesive region, the peel energy was linearly dependent on the MA concentration, up to an optimal concentration of approximately 1 mol%. Beyond this quantity, the peel energy decreases substantially and has a cohesive mode of failure. This behavior is similar to previous research that used model carboxylated poly(butadiene) and can be interpreted based on the surface re-structuring polymer-solid interface models developed by Lee and Gong *et al.* Using this fundamental understanding of the adhesion properties, the peel energy and mode of failure can be designed and controlled. This work could be extended by the incorporation of several different functional groups to enhance the adhesive properties of the polymer towards a variety of substrates.

The bio-based PSAs developed in this work, while having similar adhesion and mechanical properties to their petroleum based PSA, differ substantially in the following attributes: the fatty acid based PSA are both biodegradable and biocompatible. The biocompatibility to human tissue and blood cells was determined by Klapperich *et al.* at Boston University [25] and the biodegradability was examined by Zhu and Wool [26]. The fatty acid based PSA were found to degrade slowly in soil burial experiments (10% weight loss in four months) and were non-toxic to human cells, using the MTT cytotoxicity assay. The new bio-based PSA may have particular utility in the medical field while providing an environmentally friendly alternative to many of the disposable PSA products used in our daily lives.

ACKNOWLEDGMENTS

The authors are grateful to the Hercules Corporation of Wilmington Delaware and the United States Department of Agriculture–National Research Initiative (USDA-NRI) program for financial support of this research with Grant No. 2005–35504–16137. We acknowledge the Adhesion Society Award to Professor Liliane Léger and thank her and her colleagues, Pierre-Gilles DeGennes and Francoise Brochard at the College de France for their advice, collegiality, and wisdom in this field over the years. Appreciation is expressed to Dr. Steven H. McKnight for his assistance with the ARXPS experiments at the Army Research Laboratory in Aberdeen, MD.

REFERENCES

[1] Khot, S. N., LaScala, J. J., Can, E., Morye, S. S., Williams, G. I., Palmese, G. R., Kusefoglu, S. H., and Wool, R. P., *J. Appl. Polym. Sci.* **82**(3), 703–722 (2001).

[2] Wool, R. P. and Sun, X. S., *Bio-Based Polymers and Composites* (Elsevier, Burlington, MA, USA, 2005).
[3] Bunker, S. P. and Wool, R. P., *J. Polym. Sci. Part A, Polym. Chem.* **40**, 451–458 (2001).
[4] Bunker, S. P., Staller, C., Willenbacher, N., and Wool, R. P., *International Journal of Adhesion and Adhesives* **23**, 29–43 (2003).
[5] Bunker, S. P., "The Synthesis and Characterization of Pressure Sensitive Adhesives from Fatty Acid Methyl Esters," Ph.D. Thesis, University of Delaware, Newark, Delware (2002).
[6] Lee, I. and Wool, R. P., *J. Polym. Sci. Part B, Polym. Phys.* **40**, 2343–2353 (2002).
[7] Lee, I. and Wool, R. P., *Macromolecules* **33**, 2680–2687 (2000).
[8] Gong, L., Wool, R. P., Friend, A. D., and Goranov, K., *J. Polym. Sci., Part A, Polym. Chem.* **37**, 3129–3137 (1999).
[9] Gong, L., Friend, A. D., and Wool, R. P., *Macromolecules* **31**(11), 3706–3714 (1998).
[10] Gong, L. and Wool, R. P., *J. Adhesion* **71**, 189–209 (1999).
[11] Gong, L., "*Polymer-Solid Interfaces: Structure and Strength,*" Ph.D. Thesis, University of Delaware, Newark, Delware (2000).
[12] Amouroux, N. and Leger, L., *J. Adhesion* **82**(9), 919–934 (2006).
[13] Leger, L. and Amouroux, N., *J. Adhesion* **81**(10–11), 1075–1085 (2005).
[14] Deruelle, M., Leger, L., and Tirrell, M., *Macromolecules* **28**, 7419–7431 (1995).
[15] Brochard-Wyart, F., DeGennes, P.-G., Leger, L., Marciano, Y., and Raphael, E., *J. Phys. Chem.* **98**, 9405–9417 (1994).
[16] Wool, R. P., *C. R. Chimie* **9**, 25 (2006); errata: **9**(1), 25–44 (2006).
[17] Wool, R. P., *J. Polym. Sci., Part B: Polym. Phys.* **43**, 168–183 (2005).
[18] Wool, R. P., *Macromolecules* **26**, 1564–1578 (1993).
[19] Wool, R. P., Bailey, D., and Friend, A. D., *J. Adhesion Sci. and Technol.* **10**, 305–316 (1996).
[20] Wool, R. P., *Polymer Interfaces: Structure and Strength* (Hanser/Gardner, 1995).
[21] McLeish, M., Plummer, M., and Donald, A., *Polymer* **30**, 1651–1661 (1989).
[22] Creton, C. and Kramer, E. J., *Macromolecules* **24**, 1846–1855 (1991).
[23] Creton, C., Kramer, E. J., Brown, H. R., *et al. Adv. Polym. Sci.* **156**, 53–177 (2002).
[24] Fetters, L. J., Lohse, D. J., Richter, D., Witten, T. A., and Zirkel, A., *Macromolecules* **27**(14) 4639–4654 (1994).
[25] Klapperich, C. M., Wool, R. P., Zhu, L., and Bonnaillie, L. M., *Proceedings of the Biomaterials Annual Meeting*, Pittsburgh, PA (2006); paper submitted for publication.
[26] Zhu, L. and Wool, R. P., *Polymer* **47**(24), 8106–8115 (2006).